

NON-INVASIVE MEASUREMENT OF DEEP TISSUE TEMPERATURE CHANGES CAUSED BY APOPTOSIS DURING BREAST CANCER NEOADJUVANT CHEMOTHERAPY: A CASE STUDY

SO HYUN CHUNG

*Department of Physics and Astronomy, University of Pennsylvania
209 S. 33rd St, Philadelphia, PA 19104, USA
sochung@sas.upenn.edu*

RITA MEHTA

*Department of Medicine, UC Irvine Healthcare
101 The City Drive South, Orange, CA 92868, USA
rsmehtha@uci.edu*

BRUCE J. TROMBERG

*Beckman Laser Institute, Department of Biomedical Engineering
University of California, Irvine, 1002 Health Sciences Rd
Irvine, CA 92612, USA
bjtrombe@uci.edu*

A. G. YODH

*Department of Physics and Astronomy, University of Pennsylvania
209 S. 33rd St, Philadelphia, PA 19104, USA
yodh@physics.upenn.edu*

Accepted 7 July 2011

Treatment-induced apoptosis of cancer cells is one goal of cancer therapy. Interestingly, more heat is generated by mitochondria during apoptosis, especially the uncoupled apoptotic state,^{1,2} compared to the resting state. In this case study, we explore these thermal effects by longitudinally measuring temperature variations in a breast lesion of a pathological complete responder during neoadjuvant chemotherapy (NAC). Diffuse Optical Spectroscopic Imaging (DOSI) was employed to derive absolute deep tissue temperature using subtle spectral features of the water peak at 975 nm.³ A significant temperature increase was observed in time windows during the anthracycline and cyclophosphamide (AC) regimen but not in the paclitaxel and bevacizumab regimen. Hemoglobin concentration changes generally did not follow temperature, suggesting the measured temperature increases were likely due to mitochondrial uncoupling rather than a direct vascular effect. A simultaneous increase of tissue oxygen saturation with temperature was observed, suggesting that oxidative stress also contributes to apoptosis. Although preliminary, this study indicates longitudinal DOSI tissue temperature monitoring

provides information that can improve our understanding of the mechanisms of tissue response during NAC.

Keywords: Deep tissue temperature; Diffuse Optical Spectroscopic Imaging; apoptosis; neoadjuvant chemotherapy; breast cancer; Bound Water Index; NIR water absorption spectrum.

1. Introduction

The metabolism of mitochondria can be monitored by measuring its thermogenic activity. Mitochondrial heating rate, for example, has been correlated with the rate of oxygen utilization during NADH oxidation.⁴ Moreover, in an experiment using isolated rat liver mitochondria,¹ heat generation has been observed to increase four-fold in the uncoupled apoptotic state compared to resting state of mitochondria, due to increased enthalpy during hydrolysis of ATP. In the uncoupled apoptotic state, the formation of mitochondrial permeability pores permits efflux of cations and larger molecules and, in the highest conductance state, this phenomena can cause loss of mitochondrial membrane potential, swelling of membrane, and uncoupling of oxidative phosphorylation. The swelling disrupts the membrane and causes the release of protons and soluble membrane protein.⁵ Additionally, during apoptosis, more numerous and smaller mitochondria are produced,⁶ an effect which at least in part can explain the increased heat generation. A successful anticancer drug based on these effects would cause uncoupling of mitochondria, which in turn could lead to apoptosis by opening ion channel pores or increasing mitochondrial membrane permeability.⁷ In this contribution, we explore these thermal effects by measuring temperature variations in a breast lesion of a pathological complete responder longitudinally during neoadjuvant chemotherapy (NAC).

We employ Diffuse Optical Spectroscopic Imaging (DOSI) to measure deep tissue temperature, using spectral features of the water absorption peak around 975 nm.³ Scattering-corrected absorption spectra exhibit subtle spectral shifts and broadening of the water peak due to both bound water and temperature variation. Recently, Chung *et al.* have demonstrated a method that employs bound water-corrected absorption spectra to measure absolute tissue temperature.³ Using this method, DOSI has exhibited temperature sensitivity similar to that of a thermistor and has been validated for *in vivo* deep tissue measurement in humans.^{8–12} Here we employ DOSI to monitor absolute temperature of a breast with an infiltrating ductal carcinoma (IDC), and we concurrently measure oxy- and deoxy-hemoglobin concentrations in these same tissues. The experiments suggest that the measured changes are caused by apoptosis during NAC.

2. Subject and Methods

2.1. Subject

A 63-year-old subject with an IDC in both breasts was measured. The patient had a tumor of about 40 mm in size (i.e., the longest axis as measured by ultrasound and mammography) at 7 o'clock, 9 cm from the nipple in her left breast; the left breast is measured in this study. The patient received NAC with two different regimens: Adriamycin

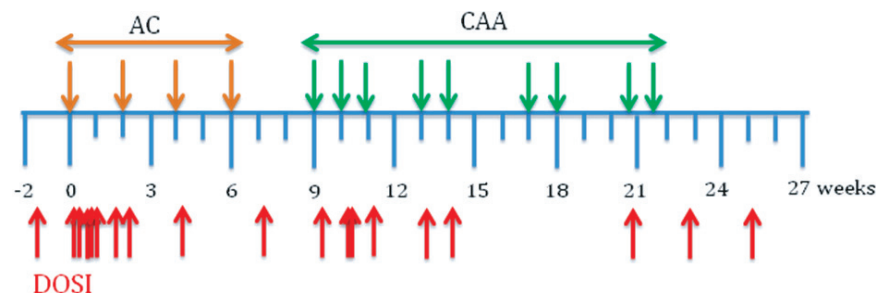


Fig. 1. NAC and DOSI monitoring schedule. Orange arrows: AC dosage; Green arrows: CAA dosage; Red arrows: DOSI measurements.

(anthracycline) + Cytoxan (cyclophosphamide) (AC, one-and-a-half months) and Carboplatin + Albumin-bound paclitaxel + Avastin (Bevacizumab) (CAA, three months). The patient was measured 19 times during the course of therapy: at a pre-treatment time (13 days before the first chemotherapy), at 8 points during AC (day 1, 2, 5, 6, 7, 12, 15 and 29 post the first chemotherapy), at 1 point in between AC and CAA (day 50) at 8 points during CAA (day 65, 71, 72, 78, 92, 99, 146 and 153), and after completion of therapy (day 175) (Fig. 1). The patient was a pathological complete responder.

2.2. Methods

DOSI employs low power near-infrared light to quantify optical and physiological properties of tissues. The diffusion model affords quantitative determination of tissue chromophore absorption spectra by separating scattering from absorption. A detailed description of the DOSI system employed in this study has been given in previous publications.^{3,8,11–13} Briefly, DOSI combines multimodulation frequency (50–600 MHz), frequency-domain photon migration (FDPM) with broadband steady-state (SS) spectroscopy. FDPM employs a model-based analysis

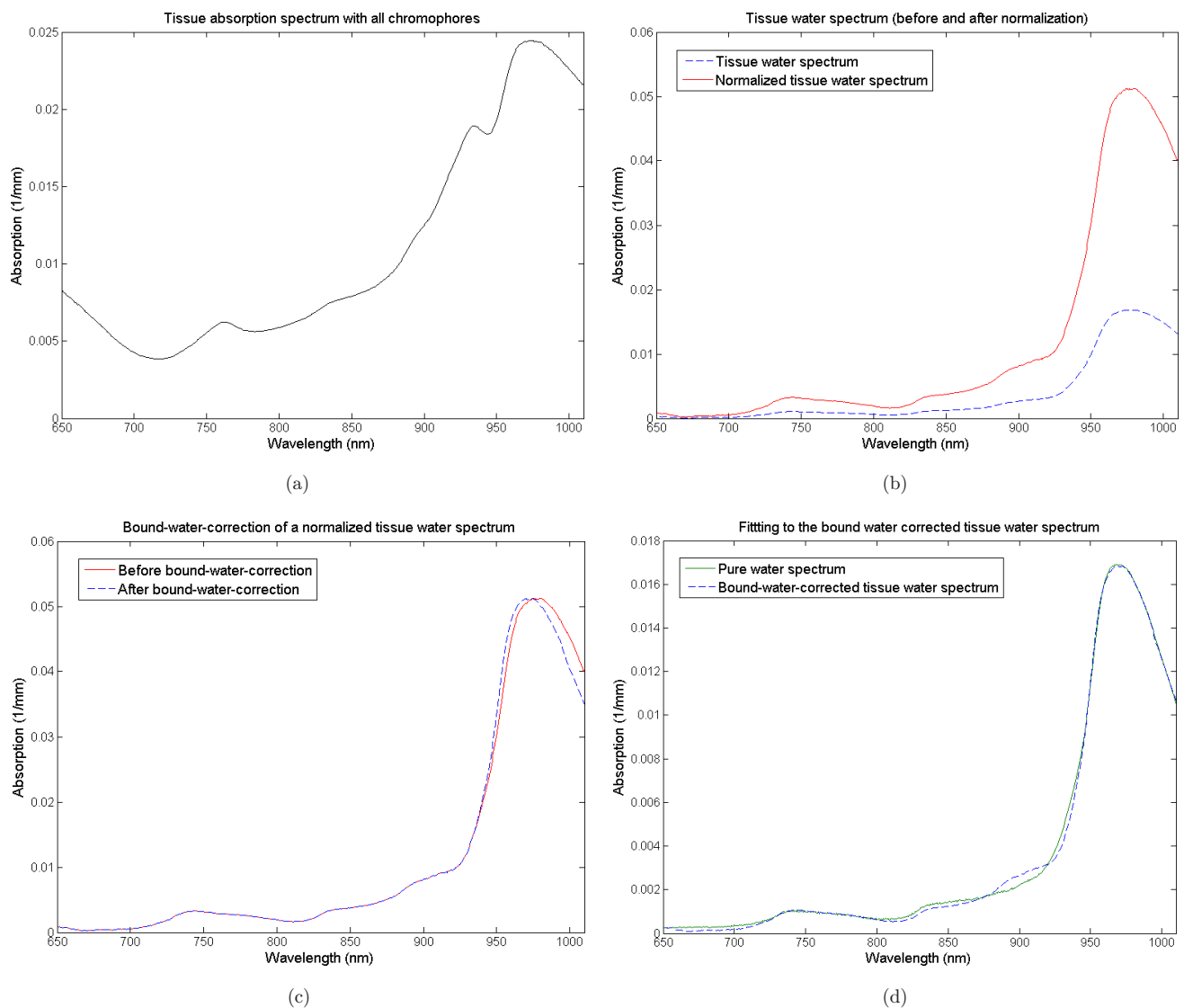


Fig. 2. Tissue temperature estimation procedure. (a) Breast tissue absorption spectrum (from areola); (b) Spectrum after removal of the contributions of all chromophores except water (dashed blue) and after subsequent normalization (solid red); (c) Normalized tissue water spectrum before (solid red) and after (dashed blue) bound-water-correction by blue-shifting; (d) Fit of a pure water spectrum to the “bound-water-corrected tissue water spectrum”.

(i.e., the diffusion approximation in the semi-infinite geometry with extrapolated zero boundary conditions) to quantify tissue absorption (μ_a) and scattering (μ'_s) parameters at discrete wavelengths.^{14–17} The μ'_s derived at each wavelength (658, 682, 785, 810, 830 and 850 nm) is fit to Mie theory to derive a continuous wavelength-dependent prediction of the tissue-scattering parameter.¹⁸ Using the so-determined μ'_s , we readily extract a continuous tissue absorption spectrum from the broadband SS reflectance data. The scattering-separated absorption spectrum from 650 to 1010 nm reveals features of the water absorption that are utilized for the temperature calculation.³ Major tissue chromophore concentrations such as oxy- and deoxy-hemoglobin (ctHbO₂ and ctHb, respectively), lipid (ctLipid), and tissue oxygen saturation ($StO_2 = ctHbO_2 / (ctHbO_2 + ctHb) \times 100$) were also derived from these tissue absorption spectra.

The instrument response functions were calibrated using tissue-simulating phantoms for FDPM and a spectraflect-coated reflectance phantom with known scattering and absorption values for broadband SS measurements as described in Cerussi *et al.*⁸ The source-detector separation for all measurements was 29 mm.

2.3. Deep tissue temperature measurement

The water peak appears between 935 and 1010 nm, and it provides information about tissue water state, water concentration, and absolute temperature.^{3,11}

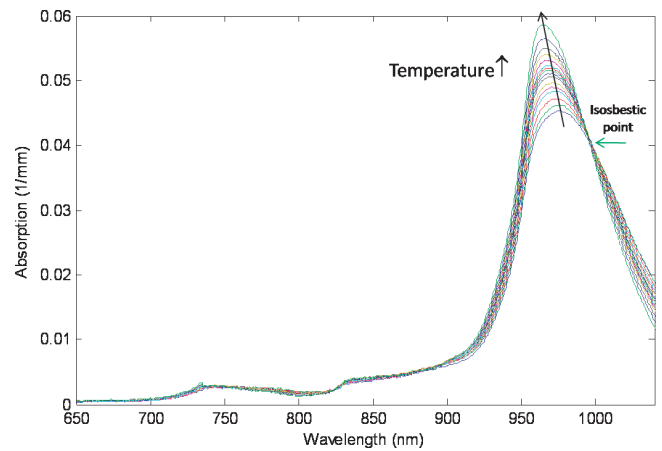


Fig. 3. Free water absorption spectra measured as a function of temperature (15°–65°C). An isosbestic point at 996 nm is clearly observed. (Reprinted with permission from *Phys. Biol. Med.* doi: 10.1088/0031-9155/53/23/005).

The effect of bound water on the peak was removed by spectral processing as explained in detail in Chung *et al.*³ Briefly, starting with the “total” tissue absorption spectrum (Fig. 2(a)), the contributions from other chromophores (oxy- and deoxy-hemoglobin, lipid and baseline-offset) were removed by subtracting their distinct spectra (i.e., chromophore extinction coefficient spectra times chromophore concentration) (Fig. 2(b) dashed-blue). The remaining “tissue water spectrum” was then normalized by a multiplicative constant so that the peak of the “tissue water spectrum” matched that of the pure water spectrum (Fig. 2(b) red). We then correct for bound water effects, which appear as broadening

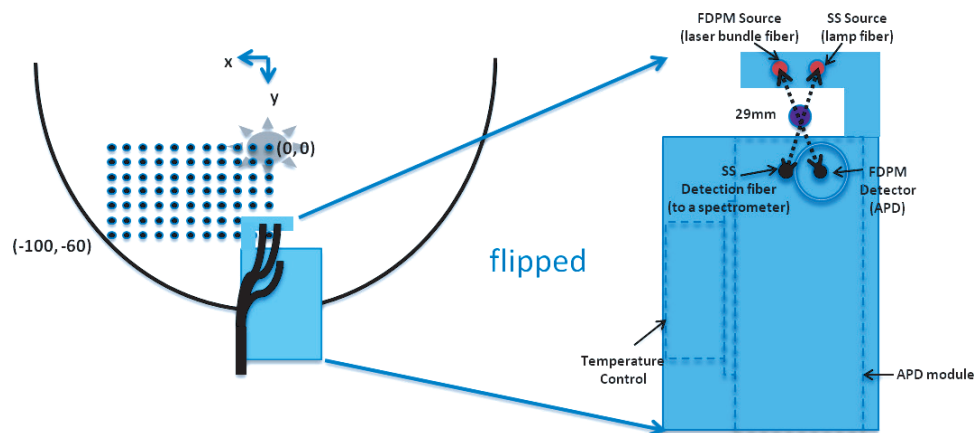


Fig. 4. Diagram showing scanning points on the lower inner quadrant of the left breast and the geometry of the hand-held probe. (0, 0) indicates where the nipple is. The purple circle on the right diagram is a mark for the measurement point made with a surgical marker.

of the water peak; in particular the “normalized tissue water spectrum” between 935 and 1010 nm was linearly blue-shifted (Fig. 2(c)) until its absorption at 996 nm (i.e., at the isosbestic point) is the same as that of pure water at 996 nm (Fig. 3). Finally, the bound-water-corrected water spectrum was “de-normalized” by the reciprocal of the normalizing multiplicative constant. The result is a “bound-water-corrected tissue water spectrum” (Fig. 2(d)). This resultant spectrum is fit to the water spectrum library at varying temperatures to determine a “best-fit” tissue temperature.

2.4. Spectroscopic images

Figure 4 illustrates how the hand-held probe is used to measure multiple locations on the left breast. All points were used to form a spectroscopic image of the lower inner quadrant of the left breast (77 points, 11×7), and to calculate averages of the underlying tissue temperature and tissue chromophore concentrations. In order to generate “smoothed” spectroscopic images, linear interpolation was used to

assign values in between the discrete measurements (taken in 1-cm increments).¹⁹ Temperature variations for the subject were determined from the full spectroscopic images of the lesion breast at each time point during NAC (Fig. 1). The lesion size, measured by ultrasound, varied during therapy. Approximately two months before NAC began, the lesion was 40 mm (longest axis, by ultrasound and mammography), and a month before starting it was 34 mm by PET-CT. The breast had high density plus multiple, scattered punctate-calcifications. After all AC doses, the size of the lesion shrunk to 17 mm. Due to these dynamic size changes and the relative movement of the tumor in the field of view, an average value of all spatial points, including both lesion and normal tissues, was used to monitor and assign a value for tissue temperature variation during therapy.

3. Results

Figure 5 shows temperature changes of the subject’s left breast during NAC. All images are derived from

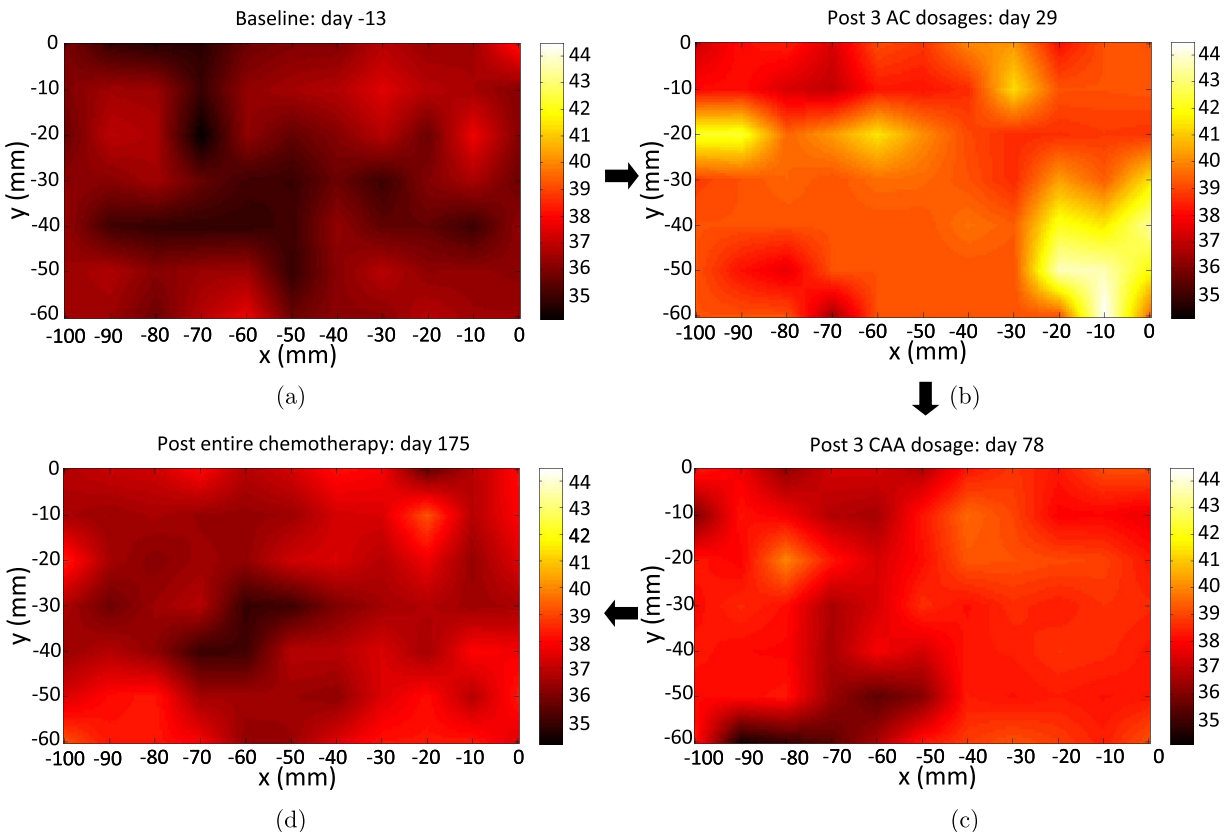


Fig. 5. DOSI images of temperature variation in a lesion breast during NAC. In clockwise order: (a) baseline, (b) after three doses of AC, (c) after three doses of CAA, (d) after completion of therapy. The color bar indicates temperature in degree Celsius.

the lower left inner quadrant of the left breast. The point (0,0) is at the nipple; from the nipple, the vertical scan extends from 0 to -60 mm and the horizontal scan extends from 0 to -100 mm. The image (a) is derived 13 days prior to the beginning of the therapy (baseline), (b) is post three doses of AC (first regimen), (c) is after three doses of CAA

(second regimen), and (d) is after completion of the entire therapy. The average tissue temperature \pm standard deviation is derived using all the points on each image (i.e., $N = 77$ for each image); these temperatures are $36 \pm 0.6^\circ\text{C}$, $39.5 \pm 1.2^\circ\text{C}$, $38 \pm 0.8^\circ\text{C}$ and $36.9 \pm 0.7^\circ\text{C}$, respectively. The patient had a core temperature measurement of 36.6°C .

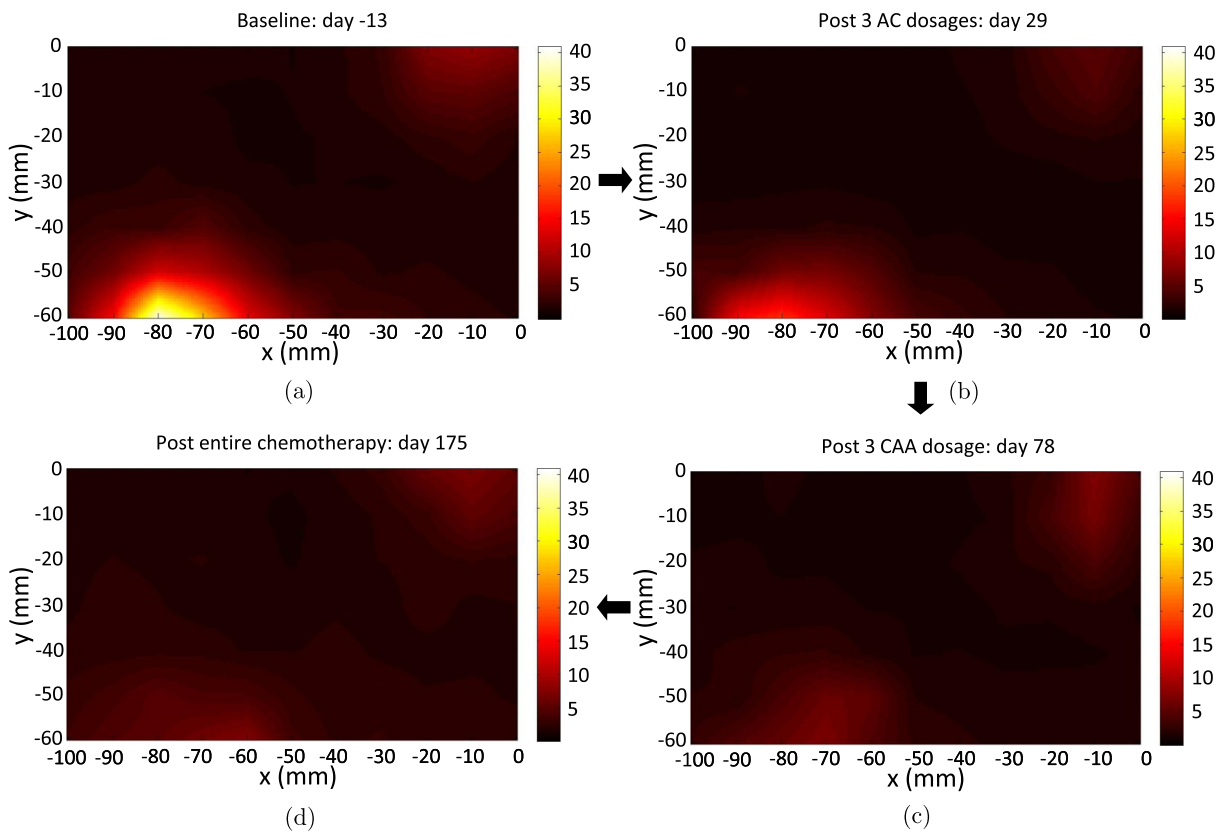


Fig. 6. TOI images at the same time points measured as the temperature images in Fig. 5. In clockwise order: (a) baseline, (b) after three doses of AC, (c) after three doses of CAA, (d) after completion of the therapy. The color bar is the contrast of TOI = (ctHb \times ctH₂O/ctLipid).

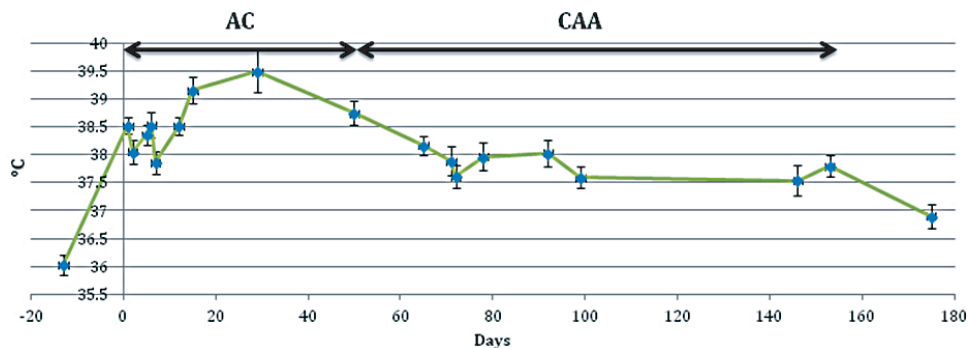


Fig. 7. Temperature change during NAC. All the points on a spectroscopic image were averaged to get blue points. Error bars represent \pm twice-the-standard-error for the points in the image, which gives a 95% confidence interval.

Figure 6 shows the spatio-temporal variation of a Tissue Optical Index (TOI), $TOI = ctHbO_2 \times ctH_2O / ctLipid$. The TOI is a combined parameter for cancer contrast,^{8,11} derived at the same time points as shown in Fig. 5. High contrast is seen in the lower left corner

of the images. The area with modest increased contrast in upper right corner is where the areola/nipple is located. Size shrinkage of the tumor is observed throughout the therapy, which was also shown in ultrasound and mammogram images.

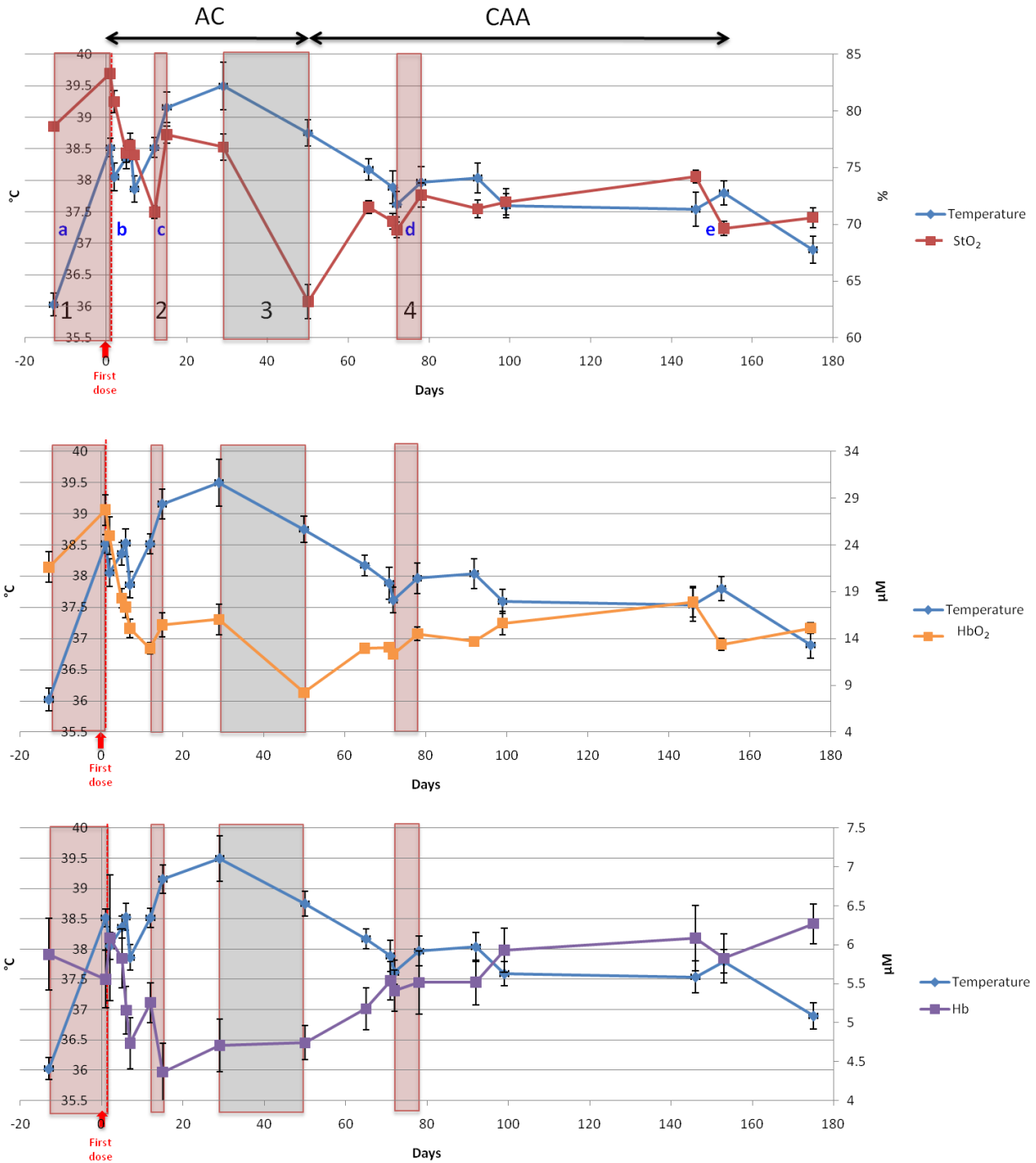


Fig. 8. Tissue oxygen saturation, oxy- and deoxy-hemoglobin and temperature changes during NAC. The red windows highlight periods wherein an increase of both temperature and StO₂ were observed, possibly due to apoptosis. The gray window highlights periods wherein a large decrease of temperature and StO₂ were observed, potentially due to massive cell death. The temperature variation rate per day was evaluated for two-point time intervals denoted by a, b, c, d and e, wherein increase of temperature was observed. Error bars represent \pm twice-the-standard-error for the points in the image, which gives a 95% confidence interval.

Longitudinal measurements of average tissue temperature are shown in Fig. 7. Each blue point is an average of all points in the image (total 77 points) and the error bars indicate \pm twice-the-standard-error for the points in the image, which gives a 95% confidence interval.²⁰ The average tissue temperature increased with some fluctuations during AC therapy. The range of variation is from 36.0 to 39.5°C, and the difference, 3.5°C, was selected as our definition of “100% temperature variation” in following text. In the following we describe variations as a percent of this maximum temperature change. During CAA, tissue temperature generally decreased. After completion of therapy (i.e., the last DOSI measurement), the average tissue temperature was $36.9 \pm 0.7^\circ\text{C}$.

Tissue oxygen saturation (StO_2) and tissue oxy- and deoxy-hemoglobin concentration (ctHbO_2 and ctHb) are plotted along with tissue temperature in Fig. 8. A rapid increase of both temperature and StO_2 was observed in the beginning of therapy (window 1). In window 1, overall consumption of oxygen decreased; this decrease might be due to cell death, as indicated by a decrease of ctHb and an

accompanying increase in ctHbO_2 . Hypoxia with fluctuating temperature followed, and then another concurrent period of rapid increase of both temperature and StO_2 was observed (window 2), with a decrease of oxygen consumption similar to that observed in window 1. After a rather slow increase of temperature between windows 2 and 3, an overall gentle decrease of temperature was observed during the rest of therapy with exception during a few periods such as in window 4 (with an accompanying increase of StO_2). However in this case (window 4), both oxy- and deoxy-Hb increased. In window 3, a large decrease of StO_2 was accompanied by a decrease in temperature.

Building on ideas from previous observations about heat generation during apoptosis,¹ we studied the rate of increase of temperature during selected time frames over the course of the therapy (Fig. 9). At the beginning of the therapy, for example, the temperature increased rapidly at about 5.1%-of-maximum per day ((a) in Fig. 7). Then during the AC dose, a large increase of temperature was observed (3.4%-of-max in (b) and 6.1%-of-max in (c)). The temperature increase during the CAA

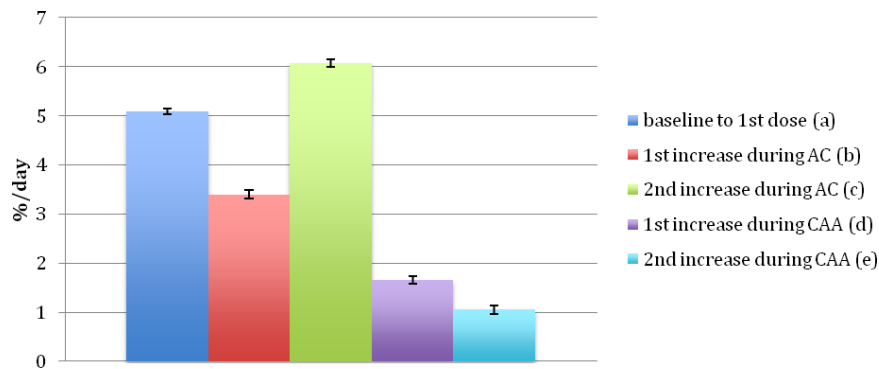


Fig. 9. Temperature increase rate at a, b, c, d, and e in Fig. 8.

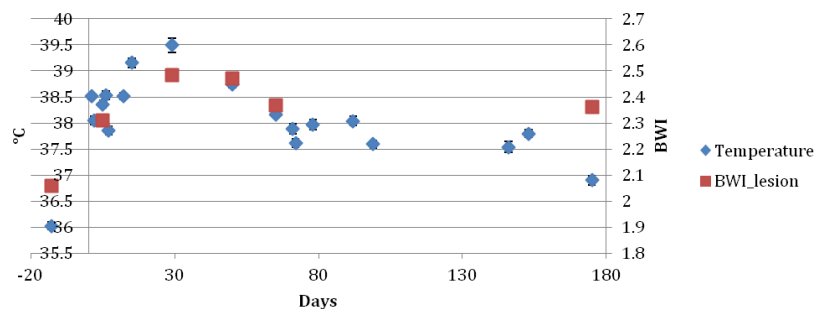


Fig. 10. Bound water index and temperature of a lesion breast measured during NAC.

was smaller: $\sim 1.7\%$ and 1.1% -of-max for (d) and (e), respectively.

4. Discussion

We have monitored tissue temperature and tissue oxygen saturation changes in a lesion-bearing breast during NAC using DOSI. The temperature patterns on the DOSI images are heterogeneous, and it is difficult to follow cancer size variation during the NAC using temperature images. Although a higher temperature was measured in the lower left corner of the scanning region wherein TOI contrast was also higher (i.e., $36.5 \pm 0.6^\circ\text{C}$ versus $36.0 \pm 0.6^\circ\text{C}$), the contrast was not large. The small contrast observed during the NAC might be a result of the fact that cells of normal tissues also experience apoptosis due to the systemic therapy. Additionally, this observation of small contrast might be, in part, due to heat transfer into the surrounding tissues and to the distribution of vascular structures in the breast.²¹ Especially in fast-growing cancers, the increase in temperature due to high metabolism and blood flow might also be expected to extend substantially beyond the margins of the tumor.^{21,22} Our subject's tumor had a high grade (8 out of 9 Nottingham Bloom-Richardson score) and was large (initially about 4 cm in the longest dimension). Gautherie has pointed out that in tumors larger than 4 cm in diameter with rapid growth rates, thermal conductivity and blood flow is very high at the periphery and in the vicinity of tumor, but decreases at the tumor center, especially when fibrotic or necrotic areas are found at histologic examination.²¹ In the future, it will be desirable to explore correlations between blood flow and temperature increases using Diffusion Correlation Spectroscopy¹⁷ and DOSI.

Higher temperature in cancer has been measured using IR thermography, liquid crystal thermography, and a fine-needle thermistor.^{21,23} Temperature changes as small as 0.3°C in cancer tissue relative to the mean thermal level of the breast provide high contrast in liquid crystal thermographic images. In IR images, a $1\text{--}2^\circ\text{C}$ temperature increase in cancer tissues were measured on skin.^{23,24} Eventually, DOSI measurements of temperature in cancer compared to normal tissues will be carried out in more patients with normal contralateral breast. The present study takes a step in this direction (although the single subject of this case

study had bi-lateral breast cancer). DOSI measured temperature variation was comparable to a previous breast cancer study using a fine-needle thermistor that observed temperature range from 35 to 37.5°C .²¹ Although the average baseline temperature of our subject ($36.0 \pm 0.6^\circ\text{C}$) was slightly lower than expected, our patient had low core temperature (36.6°C), and, in general, breast temperature is less than core temperature due to location and the presence of fat.

Previous work has found that once chemotherapy begins, patients experience fever and/or chills during or shortly after the first infusion as a result of tissue temperature increase.²⁵ In a study of 176 subjects, 16% of patients had core temperature increases to higher than 38°C after infusion, and 10% of 209 patients had temperature increases higher than 38°C after the loading dose only.²⁵ Thus, the initial temperature increase we have measured by DOSI appears consistent with other research. There is a possibility that the first temperature increase rate is bigger than 5%/day, since the first temperature increase after chemotherapy could be from a mixed reaction to the first chemodrug infusion, e.g., such as cell death due to apoptosis or inflammation.

After the NAC was completed (post 23 days), the temperature did not recover to baseline. Equivalently, 22 days after completion of the first regimen, i.e., AC (day 50 measurement), the temperature did not decrease to baseline. This temperature effect is possibly due to delayed clearance of the chemotherapy agents, since several patients still experience side-effects from NAC for more than a month after completion of therapy.

The rate of temperature increase observed in (a) and (c) of Fig. 8, during AC doses, was more than four times the variation observed after completion of the therapy (i.e., 5.1%-of-max per day in (a), 6.1%-of-max per day in (b) compared to 1.2%-of-max per day after completion of the therapy). Note, in (a) and (c), total hemoglobin concentration (i.e., the sum of deoxy- and oxy-hemoglobin concentration) also increased but with a slow rate (i.e., 2 and 2.6%, respectively). In total, the observations suggest that the difference between temperature and total hemoglobin concentration response is probably due to mitochondria uncoupling. Poe and Estabrook measured a four-fold increase in the rate of mitochondrial thermogenesis in the uncoupled apoptotic State 3u compared to the resting State 1

by measuring generated heat per minute in a Dewar containing rat liver mitochondria, using a differential calorimeter.^{1,2} They corroborated this result by adding the protonophore, dinitrophenol (DNP), to generate uncoupling of the mitochondria. This increase in heat generation was suggested to be due to the heat evolved during hydrolysis of the ATP present in the uncoupled apoptotic state, which generates twice as much heat as oxidative phosphorylation.^{1,26,27} Thus, the approximately four-fold rate of temperature increase during AC therapy measured in our study may be closely related to thermogenesis during the uncoupled apoptotic state.

Additionally, the concurrent increase of tissue oxygen saturation and decrease of Hb concentration during AC periods of rapid temperature increase indicate that oxygen uptake by tissue was diminished during these periods. This observation suggests greater uncoupling, rather than oxidative phosphorylation.¹ An oxygen concentration increase during the uncoupling state promotes formation of products of reactive oxygen species (ROS), which eventually damage cellular components including DNA.^{28,29} Evidence^{30–37} that oxidative stress initiates uncoupling of mitochondria that leads to apoptosis is this: high levels of ROS open mitochondrial pores leading to maximal substrate consumption, ATP hydrolysis, and release of mitochondrial apoptosis-inducing factor. Eliminating superoxide-producing cells is a mechanism for arresting cell proliferation observed in cancer tissues.³⁸

Thus the observed increase of temperature and StO₂ suggests that uncoupling of mitochondria is occurring during NAC. The behavior in window 3 during AC (Fig. 8) might be due to massive cell death following the large amount of uncoupling in cancer tissues that occurred in windows 1 and 2. Another increase of temperature and StO₂ was observed during CAA, but its small magnitude might not have caused significant cell death. Our results are thus consistent with the notion that the AC therapy is the major cause of cancer cell death, which can ultimately lead to complete therapeutic response.

We also measured the Bound Water Index (BWI) in the lesion-bearing breast at a few time points during chemotherapy (Fig. 10). BWI generally increased with temperature as therapy progressed and the tissue returned to a more normal state.^{9–11} The correlation of BWI with temperature

may be related to apoptosis-induced changes in the tissue distribution of water-associated macromolecules and could be a consequence of uncoupling of mitochondria, membrane disruption and release of soluble membrane proteins (more than 1500 Dal) during AC dosage.⁵ The observed decrease of BWI after AC dosage (but with a value still higher than baseline) might be due to cleaning of excessive dead cells after apoptosis and remaining normal cells by phagocytes.

It is possible that there is an effect from collagen changes in the stroma, although most chemotherapy agents target cancer cells, and lipid composition increases as therapy progresses. The absorption of collagen in normal human breast tissues is very low (approximately 0.0017–0.0028 mm⁻¹ for collagen density of 100 mg/cm³)³⁹ compared to water absorption in the wavelength regime wherein the large water peak is observed. Especially in the range where the water peak shape varies noticeably with temperature (950–996 nm), the effect of collagen concentration variation is small (less than 0.1°C) based on simple simulations that assumed 20% changes in collagen composition. Furthermore, the almost perfect fit of the “final” tissue water spectrum to a pure water spectrum suggests that the collagen is not playing a significant role in our computed temperature. However, in the future it will be desirable to explore the use of the full collagen spectral features in the spectral processing algorithm for temperature estimation.

In summary, deep tissue temperature, tissue oxygen saturation, and Bound Water Index were measured non-invasively in a lesion breast of a pathological complete responder using DOSI over the course of NAC. Rapid increases of temperature and StO₂ observed in selected time windows during early-stage AC therapy are suggestive of mitochondrial thermogenesis, oxidative stress, and apoptosis. Although preliminary, the results of this case study suggest that simultaneous measurements of deep tissue temperature and StO₂ may help to reveal mechanisms of tissue response to chemotherapy and provide feedback for optimizing treatment.

Acknowledgments

SHC greatly appreciates the precious opportunity to have worked with Britton Chance on this project and particularly thanks him for guidance about

biochemical mechanisms in breast cancer. We all thank Montana Compton, who coordinated the NAC studies, and the patient volunteer. This work was supported by NIH R01-CA75124, R01-EB002109 and Susan G. Komen for the Cure Postdoctoral Fellowship provided to University of Pennsylvania, and P41-RR01192, U54-CA105480, U54CA136400, P30-CA62203 provided to University of California, Irvine. BJT reports patents, owned by the University of California, related to the technology and analysis methods described in this study. The DOSI instrumentation used in this study was constructed in a university laboratory using federal grant support (NIH). The University of California has licensed DOSI technology and analysis methods to two companies, FirstScan, Inc. and Volighten, Inc. for different fields of use, including breast cancer (FirstScan). This research was completed without participation, knowledge, or financial support of either company, and data were acquired and processed from patients by coauthors unaffiliated with either entity. The IRB and Conflict of Interest Office of the University of California, Irvine, have reviewed both patent and corporate disclosures and no concerns were found.

References

1. M. Poe, R. W. Estabrook, "Kinetic studies of temperature changes and oxygen uptake concomitant with substrate oxidation by mitochondria — Enthalpy of succinate oxidation during Atp formation by mitochondria," *Arch. Biochem. Biophys.* **126**, 320–330 (1968).
2. B. Chance, B. Schoener, "High and low energy states of cytochromes. I. In mitochondria," *J. Biol. Chem.* **241**, 4567–4573 (1966).
3. S. H. Chung, A. E. Cerussi, S. I. Merritt, J. Ruth, B. J. Tromberg, "Non-invasive tissue temperature measurements based on quantitative diffuse optical spectroscopy (DOS) of water," *Phys. Med. Biol.* **55**, 3753–3765 (2010).
4. M. Poe, H. Gutfreun, R. W. Estabrook, "Kinetic studies of temperature changes and oxygen uptake in a differential calorimeter — Heat of oxidation of NADH and succinate," *Arch. Biochem. Biophys.* **122**, 204–211 (1967).
5. C. J. Coté, J. Lerman, I. D. Todres, *A Practice of Anesthesia for Infants and Children*, p. 392, Saunders Elsevier, Philadelphia (2009).
6. D. F. Suen, K. L. Norris, R. J. Youle, "Mitochondrial dynamics and apoptosis," *Gen. Devel.* **22**, 1577–1590 (2008).
7. R. W. Johnstone, A. A. Ruefli, S. W. Lowe, "Apoptosis: A link between cancer genetics and chemotherapy," *Cell* **108**, 153–164 (2002).
8. A. E. Cerussi *et al.*, "In vivo absorption, scattering, and physiologic properties of 58 malignant breast tumors determined by broadband diffuse optical spectroscopy," *J. Biomed. Optic.* **11**, 044005 (2006).
9. S. H. Chung, A. Cerussi, R. Mehta, D. Hsiang, B. J. Tromberg, "Non-invasive detection and monitoring of tumor pathological grade during neoadjuvant chemotherapy by measuring tissue water state using diffuse optical spectroscopic imaging," *Cancer Res.* **69**, 101S–101S (2009).
10. S. H. Chung, A. E. Cerussi, D. Hsiang, B. J. Tromberg, "Non-invasive measurement of pathological heterogeneity of cancer tissues using water state information from diffuse optical spectroscopic imaging," *Cancer Res.* **69**, 767S–767S (2009).
11. S. H. Chung *et al.*, "In vivo water state measurements in breast cancer using broadband diffuse optical spectroscopy," *Phys. Med. Biol.* **53**, 6713 (2008).
12. D. Jakubowski, F. Bevilacqua, S. Merritt, A. Cerussi, B. J. Tromberg, in *Biomedical Optical Imaging*, J. G. Fujimoto, D. L. Farkas, Eds., 330–355, Oxford University Press, New York (2009).
13. F. Bevilacqua, A. J. Berger, A. E. Cerussi, D. Jakubowski, B. J. Tromberg, "Broadband absorption spectroscopy in turbid media by combined frequency-domain and steady-state methods," *Appl. Optic* **39**, 6498–6507 (2000).
14. B. J. Tromberg, L. O. Svaasand, T. T. Tsay, R. C. Haskell, "Properties of photon density waves in multiple-scattering media," *Appl. Optics* **32**, 607–616 (1993).
15. J. B. Fishkin, E. Gratton, "Propagation of photon-density waves in strongly scattering media containing an absorbing semi-infinite plane bounded by a straight edge," *J. Optic. Soc. Amer. — Optic Image Sci. Vision* **10**, 127–140 (1993).
16. R. C. Haskell, L. O. Svaasand, T. T. Tsay, T. C. Feng, M. S. Mcadams, "Boundary conditions for the diffusion equation in radiative transfer," *J. Opt. Soc. Amer. A* **11**, 2727–2741 (1994).
17. T. Durduran, R. Choe, W. B. Baker, A. G. Yodh, "Diffuse optics for tissue monitoring and tomography," *Reports Prog. Phys.* **73**, 1–43 (2010).
18. R. Graaff *et al.*, "Reduced light-scattering properties for mixtures of spherical-particles — A simple approximation derived from Mie calculations," *Appl. Opt.* **31**, 1370–1376 (1992).
19. W. Tanamai, C. Chen, S. Siavoshi, A. Cerussi, "Diffuse optical spectroscopy measurements of healing in breast tissue after core biopsy: Case study," *J. Biomed. Optic* **14**, 014024 (2009).

20. D. L. Streiner, "Maintaining standards: Differences between the standard deviation and standard error, and when to use each," *Canadian J. Psych.-Revue Canadienne De Psychiatrie* **41**, 498–502 (1996).
21. M. Gautherie, "Thermopathology of breast cancer: Measurement and analysis of *in vivo* temperature and blood flow," *Annals New York Acad. Sci.* **335**, 383–415 (1980).
22. P. M. Gullino, *In vitro Perfusion of Tumors*, J. C. Norman, Ed., pp. 877–898, Appleton-Century Crofts, New York, NY (1968).
23. J. R. Keyserlingk, P. D. Ahlgren, E. Yu, N. Bellevue, M. Yassa, "Functional infrared imaging of the breast — Historical perspectives, current applications, and future considerations," *IEEE Eng. Med. Biol. Magazine* **19**, 30–41 (2000).
24. K. L. Williams, R. S. Handley, F. J. Williams, "Infra-red thermometry in diagnosis of breast disease," *Lancet* **2**, 1378–1381 (1961).
25. M. A. Cobleigh et al., "Multinational study of the efficacy and safety of humanized anti-HER2 monoclonal antibody in women who have HER2-overexpressing metastatic breast cancer that has progressed after chemotherapy for metastatic disease," *J. Clin. Oncol.* **17**, 2639–2648 (1999).
26. B. Chance, G. R. Williams, *The Respiratory Chain and Oxidative Phosphorylation*, F. F. Nord, Ed., John Wiley and Sons, Inc., Hoboken, NJ (1956).
27. E. Gnaiger, "MitoPathways: Respiratory states and coupling control ratios," *Mitochondr. Physiol. Netw.* **12.15**, 1–12 (2010).
28. A. Boveris, B. Chance, "Mitochondrial generation of hydrogen-peroxide — General properties and effect of hyperbaric-oxygen," *Biochem. J.* **134**, 707–716 (1973).
29. S. Papa, V. P. Skulachev, "Reactive oxygen species, mitochondria, apoptosis and aging," *Molec. Cell. Biochem.* **174**, 305–319 (1997).
30. A. F. G. Slater et al., *Oxidative Stress and Apoptosis*, R. G. Cutler, L. Packer, J. Bertram, A. Mori, Eds., Birkhäuser-Verlag, Basel (1995).
31. P. X. Petit et al., "Alterations in mitochondrial structure and function are early events of dexamethasone-induced thymocyte apoptosis," *J. Cell Biol.* **130**, 157–167 (1995).
32. C. Richter, M. Schweizer, A. Cossarizza, C. Franceschi, "Control of apoptosis by the cellular ATP level," *FEBS Lett.* **378**, 107–110 (1996).
33. E. J. Wolvetang, K. L. Johnson, K. Krauer, S. J. Ralph, A. W. Linnane, "Mitochondrial respiratory-chain inhibitors induce apoptosis," *FEBS Lett.* **339**, 40–44 (1994).
34. M. Yoneda, K. Katsumata, M. Hayakawa, M. Tanaka, T. Ozawa, "Oxygen stress induces an apoptotic cell-death associated with fragmentation of mitochondrial genome," *Biochem. Biophys. Res. Commun.* **209**, 723–729 (1995).
35. N. Zamzami et al., "Inhibitors of permeability transition interfere with the disruption of the mitochondrial transmembrane potential during apoptosis," *FEBS Lett.* **384**, 53–57 (1996).
36. P. Marchetti et al., "Apoptosis-associated derangement of mitochondrial function in cells lacking mitochondrial DNA," *Cancer Res.* **56**, 2033–2038 (1996).
37. N. Zamzami et al., "Mitochondrial control of nuclear apoptosis," *J. Exp. Med.* **183**, 1533–1544 (1996).
38. J. M. Mates, F. M. Sanchez-Jimenez, "Role of reactive oxygen species in apoptosis: Implications for cancer therapy," *Int. J. Biochem. Cell Biol.* **32**, 157–170 (2000).
39. P. Taroni, D. Comelli, A. Pifferi, A. Torricelli, R. Cubeddu, "Absorption of collagen: Effects on the estimate of breast composition and related diagnostic implications," *J. Biomed. Optic* **12**, 014021 (2007).